

Highly tunable NbTiN Josephson junctions fabricated with focused helium ion beam

Aki Ruhtinas* and Ilari J. Maasilta†

Nanoscience Center, Department of Physics, University of Jyväskylä, FI-40014 Jyväskylä, Finland

(Dated: March 31, 2023)

We demonstrate a "direct writing" method for the fabrication of planar Josephson junctions from high quality superconducting niobium titanium nitride (NbTiN) thin films using focused He-ion beam irradiation. Compared to the materials previously used in such processing, YBCO and MgB₂, NbTiN has much better mechanical and electrical properties, as well as good corrosion resistance. We show that we can control the suppression of superconductivity in NbTiN as a function of the helium ion beam fluence, and that this controllable critical temperature suppression combined with the high spatial resolution and position control of the He-ion beam in a helium ion microscope enables us to successfully fabricate Josephson junctions with highly tunable weak links. Because of the continuous nature of the disorder-induced metal-insulator transition, this method allows the creation of barriers with wide range of resistivities ranging from the metallic to the insulating state, with the critical current and the junction resistance varying over two orders of magnitude. Electrical transport measurements show that junctions follow closely the ideal resistively and capacitively shunted junction behavior, have high characteristic voltages (0.2 – 1.4 mV) and show Shapiro steps up to very high orders. This suggests that these type of junctions are suitable for a wide range of applications in superconducting electronics and quantum information technology, with the bonus that a whole device can be fabricated from just a single thin film, with the excellent electrical and microwave characteristics offered by NbTiN.

INTRODUCTION

Weak disorder does not have an effect on the superconducting state [1], but for strong enough disorder, with the mean free path and the Fermi-wavelength of the same order of magnitude, a superconductor can undergo a superconductor-to-insulator transition (SIT). This quantum phase transition can be exploited in the fabrication of weak links for Josephson junctions, as changing the level of disorder can change the film properties drastically. However, to make a good junction, the disordered region needs to be defined with nanometer resolution. Although ion irradiation or ion implantation of weak links is not new idea [2], high enough spatial resolution became available with the introduction of helium ion microscope (HIM), which became commercially available only in 2007. This opened up new possibilities for nanofabrication, as with HIM one can achieve a beam diameter of ~ 0.5 nm. In the direct-write fabrication of Josephson junctions, this high resolution helium ion beam is used to locally irradiate a superconducting film to introduce disorder and therefore control the SIT, enabling fabrication of highly tunable weak links where both the width and the strength of the link can be tuned continuously. However, near the SIT, the superconducting film properties are relatively sensitive to changes in the helium ion fluence, and therefore a very precise fluence control is needed for an accurate tuning of the weak link.

In 2015, direct writing of Josephson junctions was first demonstrated in YBCO films [3]. After this, the direct writing method has been applied not only to YBCO thin films to create Josephson junctions and SQUIDS [4–6], but also to MgB₂ [7] and to Bi₂Sr₂CaCu₂O_{8+x} [8] thin films. However, these materials are often difficult to work

with, and electrical and mechanical properties are not good enough for some applications. Also for many superconducting devices, a smaller superconducting gap is desired. It is known that a disorder driven superconductor-insulator transition exists in NbN [9–11], TiN [12, 13] and NbTiN [14, 15], and thus direct writing should work in all of the materials, in principle. Consequently, there has been demonstration of direct writing of nanowires in NbN [16], and we have some preliminary experimental evidence that direct writing of Josephson junctions should work in nitrides of NbN, NbTiN and TiN [17].

Here, we focus on using NbTiN as the superconducting material, to which we direct write Josephson junctions with a helium ion microscope beam. The observed electrical characteristics of the junctions closely follow established theory. We use pulsed laser deposition (PLD) to deposit high quality NbTiN with a relatively high $T_c > 15$ K. NbTiN has good electrical and mechanical characteristics and high corrosion resistance which makes it an excellent choice for Josephson junction fabrication. Moreover, NbTiN is already a state-of-the-art material in many devices, and it has been used in microwave resonators [18, 19], rapid single flux quantum (RSFQ) devices [20], superconducting nanowire single-photon detectors (SNSPDs) [21, 22] and in THz-band heterodyne sensing technologies [23, 24]. As NbTiN is one of the most promising materials in a wide variety of applications, the ability to fabricate whole devices using only NbTiN seems to be a promising avenue to pursue.

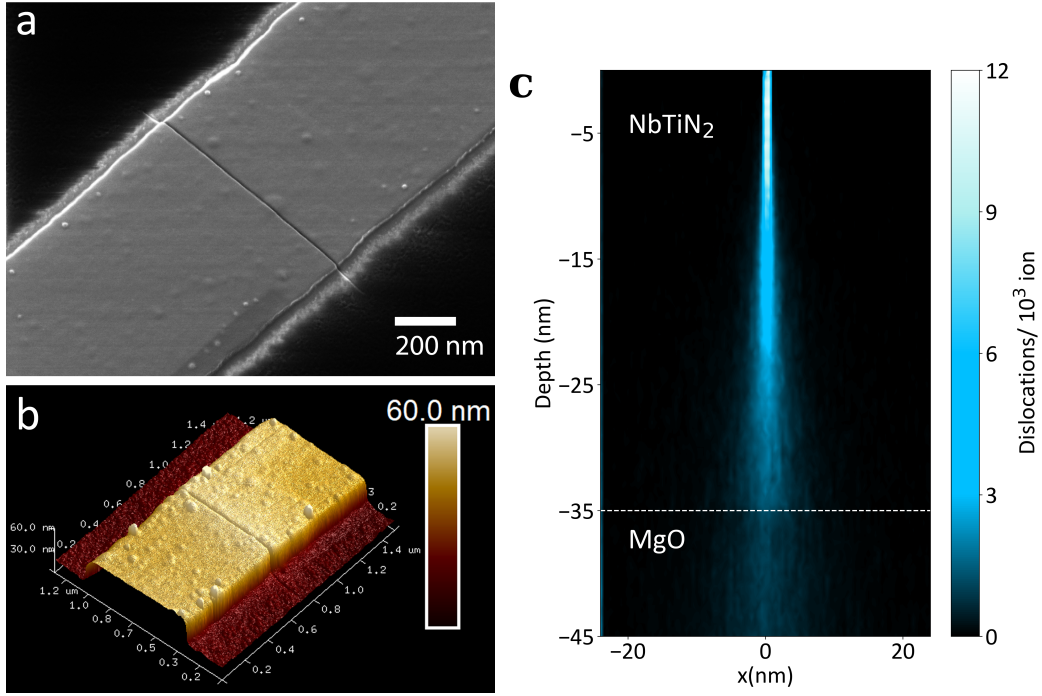


FIG. 1: (a) a helium ion micrograph and (b) an atomic force microscope (AFM) image of a Josephson junction created by helium ion irradiation. The fluence used here was $\sim 6 \cdot 10^{18}$ ion/cm². The width of the irradiated region is quite wide, ~ 14 nm, and superconducting wire is partially milled, as can be seen from both the AFM and HIM images. (c) Shows a SRIM simulation of the film dislocations due to 30 kV helium ion beam impinging to 35 nm thick NbTiN₂ target.

EXPERIMENTAL DETAILS

Pulsed laser deposition

Thin films of NbTiN were deposited using the same reactive infrared pulsed laser deposition (PLD) technique as demonstrated for TiN [25], TaN[26] and NbN[27] before. We use a Q-switched Nd:YAG laser (Ekspla NL301 HT) operating at its fundamental 1064 nm wavelength. The laser fluence at the target was ~ 6 J/cm² and the pulse repetition frequency 10 Hz. As a target, we used two 99.99% purity NbTi alloy targets (Matsurf Technologies Inc.) with two different compositions, Nb_{0.39}Ti_{0.61} and Nb_{0.5}Ti_{0.5}. The target was ablated in ultra-high purity nitrogen atmosphere using ~ 50 mTorr pressure. The substrate temperature was kept at 700 °C, and the substrates were glued to substrate heater using silver glue in order to maximize the thermal contact. The growth rate of the film was ~ 1 nm/min. As a substrate, we used cubic (100)-oriented MgO (Crystec GmbH) for several reasons. First of all, it has a good lattice match to NbTiN, allowing epitaxial growth. Second, the SF₆-based plasma etching step to define the wires stops to MgO. Third and most importantly, MgO seems to handle large helium ion fluences without issues with the formation of helium bubbles in the substrate, unlike Si, for example. The super-

conducting critical temperature of our PLD deposited NbTiN films depends on the thickness. for a 50 nm film thickness, we have obtained $T_c \sim 15$ K while the highest achieved T_c is 15.7 K for a thickness of 100 nm. For a 22 nm film, we have achieved a T_c of 11.5 K. The resistivity of the best films is ~ 30 $\mu\Omega$ m, and the superconducting transition width is typically quite narrow (~ 50 mK).

Electron beam lithography and plasma etching

Bonding pads and superconducting wires with widths ranging between 0.2-2 μ m were defined to the PLD deposited nitride film with electron beam lithography and reactive ion etching. Before the lithography, the chip was cleaned in isopropyl alcohol (IPA) bath using an ultrasonic cleaner (Finnsonic) to get rid off the silver glue residues and other contaminants. Then, a resist layer was spun on the samples at 4000 rpm for 60 s, with the resulting resist layer thickness approximately 400 nm. Here we used the negative e-beam resist AR-N 7520.17, because it has excellent plasma etch resistance and because a negative resist is more suitable for our device geometry. After spinning, an e-beam lithography tool (Raith E-Line) was used to expose the resist to define the pattern, with a 110-150 μ C/cm² dose depending on the pattern size. Af-

ter the exposure, the resist was developed in undiluted AZ 351B developer for 50s, and rinsed with IPA, and reactive ion etching (RIE) was performed (Oxford Plasmalab 80+ RIE) to remove the NbTiN film outside the wire and bonding pad regions, using 60 W RF power, 100 sccm SF_6 flow, and 5 sccm O_2 flow at a pressure of 70 mTorr. This results in etching speed of roughly 15 nm/min. Finally, the remaining resist was removed using O_2 plasma cleaning in the same RIE tool.

Helium ion irradiation and simulation

Josephson junctions were defined to the superconducting wire using a helium ion beam "direct writing" technique. For this, we used 30 kV He^+ beam in a Zeiss Orion Nanofab helium ion microscope with the nominal spatial resolution of 0.5 nm. We varied the beam parameters, but mostly we used a 20 μm aperture and a spot size of 4, resulting in a beam current of 0.5-1 pA. The junction was defined as a narrow line irradiation, perpendicular to the length of the superconducting wire, creating a weak link between the two electrodes (Figure 1). The irradiation was performed with a 1 nm step size and typically a 1000 μs dwell time for each step, with the number of repeats adjusted to get the desired fluence. Depending on the spot size and focusing, the width of the irradiated line varied between ~ 5 nm-500 nm. Larger irradiation widths were achieved by using large spot size and by defocusing the beam significantly. Compared to the He-ion beam written YBCO junctions [3], the nitride junctions in this study need roughly two orders of magnitude more fluence to suppress superconductivity. Thus, in this work a fluence in the range $10^{16} - 10^{20} \text{ He}^+/\text{cm}^2$ was used.

After the irradiation, every junction was imaged with a quick HIM scan to ensure that the junction was successfully defined and to check the resulting linewidth. When correct HIM parameters are found, the linewidth is reproducible between subsequent irradiations. Even though the ion beam current of the instrument is not as stable as an electron beam in a SEM and fluctuates over time, the time averaged current is stable enough for reproducible junction properties.

In order to get an idea of the effects of the helium ion irradiation, we used a simulation code for ion-matter interaction (SRIM) to simulate a 30 kV He^+ beam impinging on a 35 nm NbTiN film on top of a MgO substrate (Figure 1). These simulations show that most helium ions stop in the substrate (MgO) after traveling roughly 120-200 nm, and that there is only small lateral straggle when the ions travel through the NbTiN film. In Figure 1(c), we show the dislocation density in NbTiN film caused by the helium ion beam, revealing that dislocations are concentrated in very narrow region of a few nm, which is good for an accurate junction definition.

However, the true value of the disorder is probably

lower than what is shown in Figure 1 (c). This is because at room temperature, substantial amount of target damage is usually efficiently repaired by recrystallization. This effect has been demonstrated with both experiments [28] and simulations [29], and it is most prominent in metals, so a large deviation from SRIM simulations is expected in our case. In addition, SRIM assumes a perfect crystal for each impinging ion, and does not take into account sputtering and the accumulation of dislocations. Because of the complex interplay between milling and creation of disorder, we believe that only the dimensions of disordered region should be determined from these simulations.

RESULTS

Suppression of superconductivity

In order to investigate the effects of helium ion irradiation on NbTiN thin films first more generally, we have irradiated superconducting NbTiN wires with HIM, using a varying fluence and size (linewidth) of the irradiated region. For small linewidths (~ 5 nm) we used a spot size 4, whereas for large linewidths a spot size of 2 was used. Results are shown in Figure 2 (a), revealing that helium ion beam irradiation induces strong enough local disorder to suppresses superconductivity and ultimately push the irradiated region through the superconductor-insulator transition. Superconducting critical temperature suppression as a function of helium ion fluence Φ is surprisingly linear in semilogarithmic scale [Fig. 2 (b)], indicating that $T_c \propto \log(\Phi)$. This relation allows straightforward and accurate T_c control of the NbTiN film, which may be useful in different applications. We should note that while it is difficult to determine the exact width of a large area irradiation precisely (and thus the precise value of the fluence), the width fluctuations between different irradiation rounds are small, and a possible systematic error would only shift this linear dependency.

While the irradiations with small widths (~ 5 nm) have the property $T_c \propto \log(\Phi)$ at lower fluences, the presence of Josephson supercurrent makes it more difficult to determine T_c of irradiated region. However, we can use the critical supercurrent I_c as a metric, instead. With the small linewidth irradiations, there is sharp transition to insulating phase beginning around $\sim 2 \cdot 10^{18} \text{ ion}/\text{cm}^2$ for 35 nm thick films, and this transition shifts to a higher fluence ($\sim 1 \cdot 10^{19} \text{ ion}/\text{cm}^2$) for 97 nm films [Fig. 2 (b)]. This shift is expected, as there are more atoms to displace when films are thicker. However, there is a lot of energy left in He ions after traveling through the NbTiN, so that a film thickness increase does not increase the transition fluence linearly. We find that this SIT region (blue region in Figure 2 (b)) is the best for Josephson junction

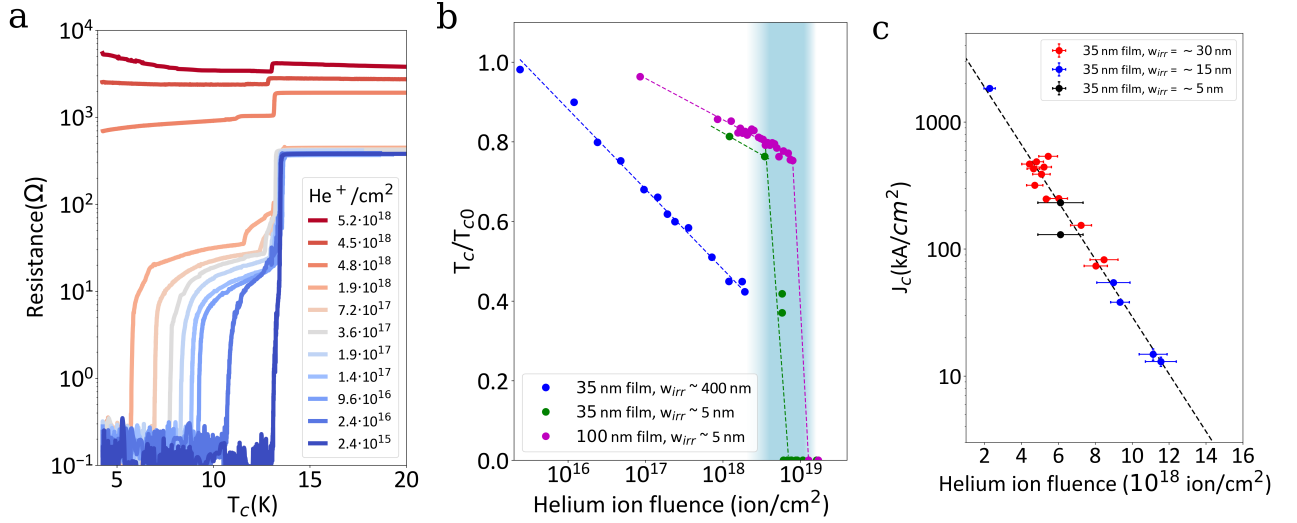


FIG. 2: Suppression of T_c and the disorder driven SIT in NbTiN thin films. Panel (a) shows the resistance of a superconducting NbTiN wire after irradiation a region of the wire with a helium ion beam using different fluences. The wire undergoes a transition from the superconducting to the insulating phase as the helium ion fluence increases, with a suppression of T_c along the way. Panel (b) shows the T_c of the irradiated region in a semilogarithmic plot, showing a linear dependency of T_c as a function of the logarithm of the ion beam fluence. SIT region is shaded in blue. Panel (c) shows a logarithmic dependence of the critical current density as a function of the helium ion fluence.

fabrication, as in that case the critical current can be tuned continuously from $\sim I_c$ of the bare wire down to zero. We demonstrate this in Figure 2(c), where we plot the critical current density J_c of several junctions fabricated to ~ 500 nm wide and 35 nm thick wires, where the junctions are in this SIT region. We find that J_c is exponentially proportional to the helium ion fluence, so that $\log(I_c) \propto \Phi$. Because the SIT region is relatively narrow in Φ , precise control of the helium ion beam is needed for reproducible fabrication of junctions. This is especially true for the narrowest < 10 nm junctions, as small changes in the irradiation width change Φ and thus I_c drastically.

Josephson junctions

DC transport measurements

After we characterized the SIT as a function of fluence, we proceeded to fabricate and electrically characterize weak links with varying strengths and widths. These junctions were characterized via DC transport measurements down to 1.5 K with a liquid helium evaporation cryostat. We measured the current-voltage characteristics (IVC) at different temperatures using a battery powered sweepbox and a voltage divider, to achieve a low noise level. Voltage and current were measured using Ithaco preamplifiers (models 1201 and 1211), and the differential conductance was simultaneously determined either with lock-in technique or with numerical differen-

tiation of the IVC. In Figure 3, we show DC transport measurements of four representative NbTiN Josephson junctions (JJ1-JJ4) fabricated with the direct writing method. In order to extract more precisely the critical current (I_c) and normal state resistance (R_n) values, the IVC of every junction was fitted at selected temperatures with the RCSJ model [30]. From these fits, we extracted I_c , R_n and values for the junction capacitance C . The experimental parameters of these junctions are presented in Table 1.

There are some uncertainties in the reported parameter values, as the junction length and the milling depth are difficult to experimentally estimate accurately. The length of the junction (width of the HIM irradiation region) can be estimated from HIM and AFM images with reasonable accuracy and are reported in Table 1, but the possible milling depth of the film was not directly measured. As some milling of the film can evidently occur (an example shown in Fig. 1(b)), this can distort the reported junction area A_j and J_c values in Table 1 (calculated assuming no milling), and these should be regarded as upper and lower limits, respectively.

From the transport measurements we concluded that it is possible to tune the critical current from I_c of the superconducting leads continuously down to zero, and thus I_c can be controlled over several orders of magnitude. In junctions JJ1-JJ4, I_c varies from 2.2 μ A (JJ1) to 390 μ A (JJ4). The junction dimensions such as the film thickness t , the superconducting wire width W and the junction length L_j (=irradiation width) vary between junctions JJ1-JJ4, showing flexibility of the method. JJ2

was fabricated from a 100 nm thick film, demonstrating that direct writing method is feasible for such films, thicker than the most commonly used ~ 30 nm thickness, which to our knowledge has not been reported before. In addition, we have demonstrated that fabrication of longer junctions is also possible with the direct write method, as JJ3 is 30 nm long. For that case, the resistivity of the barrier is low, but the long length limits the critical current.

Calculated resistivities for the devices (barriers) ranged from $\sim 1 \cdot 10^{-3} \Omega \text{ cm}$ (JJ4) to $\sim 2 \cdot 10^{-1} \Omega \text{ cm}$ (JJ1) (As milling of the junction was not taken into account, these are the upper limit values). However if we assume an extreme case of the film thickness milled down to 5 nm, we get only an order of magnitude smaller resistivities, still high values for metals. Sheet resistances can be calculated more accurately, and these vary between $\sim 0.3 \text{ k}\Omega$ (JJ4, JJ3) to $\sim 50 \text{ k}\Omega$ (JJ1). In all of the junctions, R_n seems to be independent of temperature, indicating still metallic conductivity. In NbTiN, a Bose metallic state has been experimentally detected when the sheet resistance is above the superconducting resistance quantum R_q [15], so that $R_\square > h/4e^2 = 6.45 \text{ k}\Omega$. When compared to the measured normal metal R_\square here, it seems that junctions JJ1 and JJ2 are in the vicinity or above this limit, suggesting a possible presence of the Bose metal phase. Sample JJ1 has high enough R_\square that based on Ref. [14] these films should already be in the insulating side of the SIT, indicating that JJ1 could possibly be an overdamped SIS junction.

From the measured $dV/dI(T, I)$ maps (Figure 3, right column) we can extract the temperature dependent critical current $I_c(T)$ that can be used to determine the barrier properties. When a barrier is strong, I_c has weak temperature dependence at low temperatures, and this gets weaker as the barrier gets stronger. This is expected, as $I_c(T)$ scales exponentially in case of transparent diffusive metallic barriers, and the saturation at low temperatures is signature of either an insulating barrier, or a very strong diffusive barrier [2]. We do not consider the clean limit here, as the barrier is highly disordered due to the irradiation.

In order to get a more quantitative analysis of $I_c(T)$, we performed numerical modeling, assuming diffusive transport through the weak link. The relevant length scales for transport through the weak link are the mean free path ℓ in the normal metal, and the normal metal coherence length ξ_N , given by [2]

$$\xi_N(T) = \sqrt{\frac{\hbar D}{2\pi k_B T}} \quad (1)$$

where D is the diffusivity. For junctions JJ1 and JJ2 we use the Kulik and Omelyanchuk theory (KO-I) for short SNS junctions in the diffusive limit [31], which applies when $\ell \ll L_j \ll \xi_N$. Within these assumptions, the supercurrent is given by

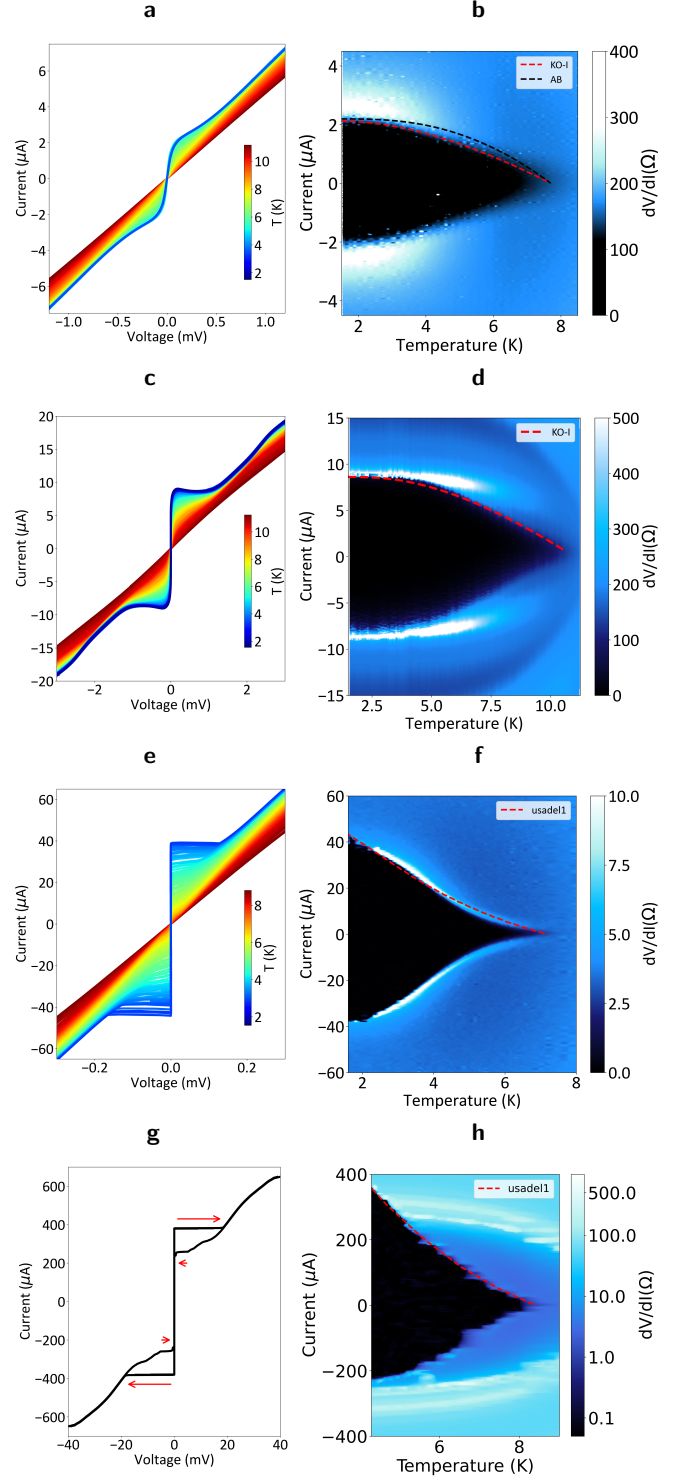


FIG. 3: DC transport measurements of four Josephson junctions fabricated using different helium ion fluences and different superconducting wire geometries devices: JJ1 (a,b), JJ2 (c,d), JJ3 (e,f) and JJ4 (g,h). Left column: current-voltage characteristics, right column: differential conductance as a function of temperature and current. For all junctions, comparison to different theories are shown in right column by the dashed lines.

JJ1 (a,b), JJ2 (c,d), JJ3 (e,f) and JJ4 (g,h). Left column: current-voltage characteristics, right column: differential conductance as a function of temperature and current. For all junctions, comparison to different theories are shown in right column by the dashed lines.

$$I(T, \varphi) = \frac{2\pi k_B T}{e R_n} \sum_{\omega_n} \frac{2\Delta \cos(\varphi/2)}{\Omega_n} \arctan \frac{\Delta \sin(\varphi/2)}{\Omega_n}, \quad (2)$$

where $\Omega_n^2 = (\hbar\omega_n)^2 + |\Delta|^2 \cos^2(\varphi/2)$, φ is the phase difference, and Matsubara frequencies ω_n are defined such that $\hbar\omega_n = \pi k_B T(2n + 1)$. The superconducting gap Δ was calculated with the BCS temperature dependence [30] and using $\Delta(T = 0) = 2k_B T_c$ that is shown to be more suitable for nitrides.

To determine $I_c(T)$, we solved Eq. 2 numerically using $\varphi = 1.25\pi/2$ and summed the Matsubara frequencies up to $n = 10^5$. The results of these calculations are shown in Figure 3 (right column) as dashed lines. For both JJ1 and JJ2, the fits to KO-I theory are very good, suggesting that these junctions are in the short diffusive limit, as one would expect from the junction dimensions and the weak link strength. For JJ1, we also compare the data to the simple Ambegaokar-Baratoff (AB) theory [32]

$$I_c(T) = \frac{\pi\Delta(T)}{2eR_n} \tanh\left(\frac{\Delta(T)}{2k_B T}\right) \quad (3)$$

valid for good SIS tunnel junctions, but we observe that the fit (black dashed line in Fig.3 (b)) is not as good as with the KO-I theory. From these measurements we can conclude that most likely the weak link is behaving more like a diffusive normal metal barrier than an insulating tunnel barrier. In addition, the assumption $\ell \ll L_j \ll \xi_N$ seems to hold very well, as the KO-I theory fits almost perfectly to the measured $I_c(T)$ s. For JJ1, the purely theoretical $I_c R_n$ value was significantly higher than the measured one, and we therefore used the prefactor $A = 0.14$ for the KO-I theory and $A = 0.18$ for the AB theory to get good fits.

For JJ2, the fitted current prefactor was $A = 0.35$ for the KO-I theory, in other words, the characteristic voltage was closer to the theoretical maximum. While the KO-I theory fits the junction JJ2 data well, it does not give as perfect a fit as for JJ1. This is most likely because the weak link in JJ2 is not as perfectly in the short junction limit. This is even more true in the case for junctions JJ3 and JJ4, where it is evident that now the approximation for a short junction is not fulfilled. With junctions JJ3 and JJ4, the length scales L_j, ξ_N are closer to each other, and the Thouless energy E_{th} defined as $E_{th} = \hbar D/L^2$ is closer to the superconducting gap Δ . In order to get theoretical predictions for I_c in junctions JJ3 and JJ4, a numerical simulation was performed using *usadel1*-code [33] that solves the quasiclassical Usadel equations in the diffusive limit. Simulation fits using this code are shown as dashed lines in Figures 3 (f) and (h). This code was also used for junctions JJ1 and JJ2, with similar results to the KO-I theory, as they are in the limit $\Delta/E_{th} \ll 1$.

The best fit to JJ3 $I_c(T)$ curve was achieved for $\Delta/E_{th} = 5$, so that $E_{th} \approx 250 \mu\text{eV}$ and $D \approx 3.4 \text{ cm}^2/\text{s}$. However, the fit was not perfect. It was possible to reproduce either the behavior at low temperatures or at high temperatures separately, but for the overall best fit a compromise was needed, as shown in Fig. 3 (f). This is probably because with D determined from fit and using Eq. 1, we get $\xi_N(8 \text{ K}) \approx 7 \text{ nm}$ and $\xi_N(1.5 \text{ K}) \approx 17 \text{ nm}$. These length scales begin to approach the junction length (30 nm) at the low temperature end, causing most likely a crossover between the short junction limit to the long junction limit as a function of T . The correction factor for I_c in the fit was $A = 0.21$, so the maximum characteristic voltage would be five times larger. Interestingly, also for all other junctions fabricated with $W_{irr} \approx 30 \text{ nm}$ and $I_c \sim 10 - 50 \mu\text{A}$, we always have a similar $I_c(T)$ behavior to JJ3, and we conclude that the $I_c(T)$ properties for JJ3 are common for these type of junctions, although not very well described with the theory.

For the junction JJ4, we found the best fit for $\Delta/E_{th} = 6$, so that we have $E_{th} \approx 240 \mu\text{eV}$, similar to the junction JJ3. As JJ4 junction was shorter, the diffusion constant is only $D \approx 0.7 \text{ cm}^2/\text{s}$ and thus $\xi_N \sim 1 - 2 \text{ nm}$ at the temperatures of the experiment. This put junction JJ4 well into the long junction limit. However, the calculated current scaling factor was $A = 1.8$, so that the measured current was almost a factor of two higher than what was expected from the simulations. This contribution is most likely due to excess current.

The characteristic voltage $I_c R_n$ values were also determined for each junction. All junctions shown in Figure 3 feature relatively high $I_c R_n$ values, ranging between $0.2 - 1.4 \text{ mV}$. From the RCSJ fits can be seen that excess current contribution in these junctions is mostly small, and for example for junction JJ3, the excess current contribution is essentially zero. This can be seen both from the RCSJ fits and the magnetotransport measurements (Figure 5), where the critical current is completely suppressed at the nodes of the Fraunhofer-pattern. The highest $I_c R_n$ junction is JJ2, which has a characteristic voltage of $\sim 1.4 \text{ mV}$. One explanation for the high value is that the sheet resistance of JJ2 is really close to R_q , and there is evidence that $I_c R_n$ for weak links closer to the phase transition are higher. Because of some non-linearity in the IVC, it is difficult to estimate the excess current precisely, but based on the RCSJ fits, its contribution should be below 10%. Hence the high $I_c R_n$ is not likely caused by an excess current contribution. The achieved $I_c R_n$ values are already suitable for example for RSFQ applications, and with some tuning it should be possible to push these characteristic voltage values even higher.

Because self-heating effects quite closely resemble capacitive effects [2, 34], the determination of capacitance from the RCSJ fits is known to be inaccurate. We believe that the hysteresis seen in junction JJ4 is most likely of

thermal origin instead of capacitive. Nevertheless, thermal effects of other junctions seem to be small, and when we take into account both the geometric and the electronic capacitance $C_e = 3\pi\hbar/(32\Delta R_n)$ [35, 36], the measured values are roughly of the same order of magnitude as the values determined from RCSJ fits. Although the above expression for the electronic capacitance is derived for tunnel junctions, this theory could be applicable here as well, as we have barriers in the vicinity of the SIT.

Microwave measurements

In order to characterize the junctions further, we performed a characterization of JJ3 with microwave irradiation. We used 2.1-11 GHz RF radiation produced with Anritsu 68367C signal generator. The minimum signal output was -10 dBm, but to get a lower power output for the measurement we used a 20 dBm attenuator in the RF line. The RF signal was carried into the cryostat via low loss coaxial cable, and the RF radiation was coupled to the sample with simple loop antenna. The microwave measurements were carried out by scanning the RF output power with a fixed frequency, and measuring dV/dI directly using a four wire lock-in technique at each power level.

For a theoretical comparison, we performed RCSJ simulations for the IV curves, and found that at 4.2 K junction behavior follows reasonably well the simpler RSJ model, which was used to simulate the RF modulated response of the junction vs. current and RF power (Shapiro map).

Figs. 4 (a) and (d) first shows examples of the IVCs of the junction JJ3 under either 6 GHz or 11 GHz RF illumination, respectively, demonstrating clearly Shapiro steps and agreement with the RSJ model simulations. The corresponding full Shapiro maps are shown in Figs. 4 (b) and (e), showing nearly ideal behavior. Comparison to the RSJ model simulated Shapiro maps (Fig. 4 (c) and (f)) show very little deviation between the experiment and the simulation, indicating a high quality junction. The Shapiro steps are visible up to high order of > 20 for the 6 GHz illumination.

Magnetic field measurements

Magnetotransport measurements were performed at 4.2 K using liquid helium dipstick and a 4 T magnet. This measurement was performed by scanning the coil current and measuring dV/dI directly using a four wire lock-in technique. For a rectangular junction geometry, the critical current is expected to follow

$$I_c(B_z) = I_{c0} \left| \frac{\sin(\pi B_z A / \phi_0)}{\pi B_z A / \phi_0} \right|, \quad (4)$$

where the junction area is $A = Lw$ and the magnetic field period for which the phase changes by 2π is $\Delta B = \phi_0/A$. For the length of the junction, the Josephson penetration depth λ_j needs to be taken into account, so that $L = L_j + 2\lambda_j$ [30]. In Figure 5, we present the results of these magnetotransport measurement for two junctions, JJ2 and JJ3. Junction JJ3, made to a $2\mu\text{m}$ wide superconducting wire has clearly a sinusoidal modulation with a vanishing critical current at the nodes. This proves that a Josephson current flows through the junction, although the pattern slightly differs from the expected $\sin(x)/x$ behaviour. Nodes are roughly equally spaced, but peculiarly, their height does not decrease monotonically as the magnetic field increases. It is known that while Equation 4 holds well for uniform current distribution and for wide ($w \gg \lambda_j$) and thick films, in planar junctions made from very thin films ($\lambda_j \gg t$) this diffraction pattern is often altered because of flux focusing effects [37]. For very narrow junctions, the usual magnetic period is replaced by $\Delta B \approx 1.84\Phi_0/w^2$, as was shown by Rosenthal et al. [37]. These flux focusing effects can cause also aperiodic node spacing, as well as nonmonotonically decreasing node height [38], as observed in JJ3. For JJ3, the observed period is $\Delta B \approx 5.8\text{ mT}$, and if we calculate the Josephson penetration depth using this and Eq. 4, we get $75 \pm 10\text{ nm}$. This differs considerably from the usual $\sim 200\text{ nm}$ reported in literature for NbTiN [39, 40]. The BCS prediction for the London penetration depth is given by

$$\lambda \approx 105\text{ nm} \sqrt{\frac{\rho(\mu\Omega\text{cm})}{T_c(K)}}, \quad (5)$$

and using this we get $\lambda \approx 150\text{ nm}$ for our best films, still a factor of two larger. However, flux focusing effects *increase* the effective length, and thus are not able to account for the discrepancy. Consequently, for junction JJ3 the Rosenthal correction for flux focusing gives a way too short node spacing ($\sim 1\text{ mT}$).

Magnetotransport measurements of junction JJ2, made from a 300 nm wide wire, did not show the expected Franhofer diffraction pattern. The critical current as a function of the applied magnetic field did not suppress completely, and the shape of the $I_c(B)$ shows additional constant residual I_c on top of diffraction pattern (Fig. 4 (b)). We surmise that this persisting I_c may be caused by random structural inhomogenities to which Josephson vortices are pinned [30, 41]. Yanson [41] showed that the shape of $I_c(H)$ is then altered to

$$I_c(H) = I_{c0} \sqrt{(1 - \gamma^2) (\sin(X)/X)^2 + \gamma^2}, \quad (6)$$

where $X = \pi H/H_0$. Structural inhomogenities are introduced to this equation by a random additional current $I_1(x)$ that is due to inhomogenities in the barrier, and by a factor N that represents the amount of structural

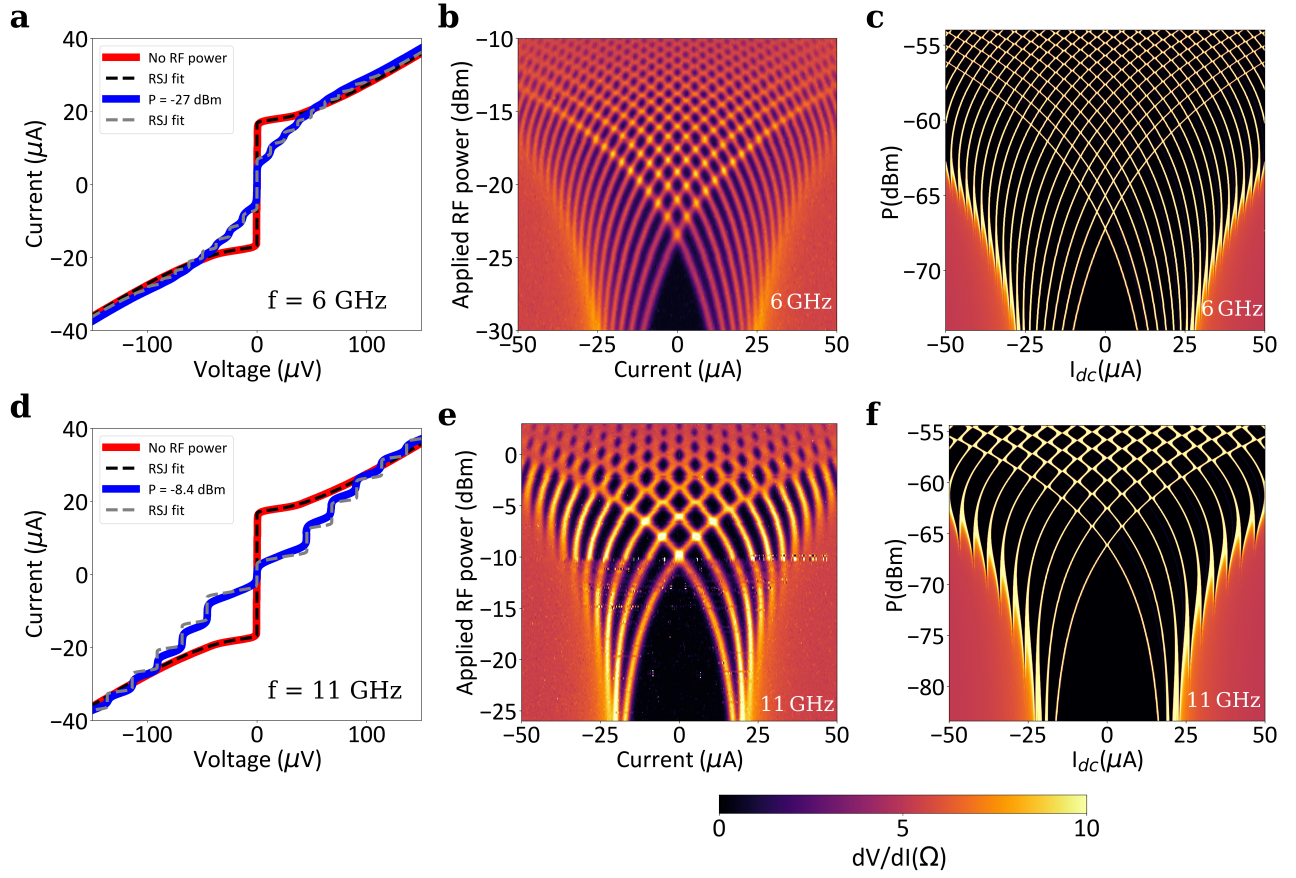


FIG. 4: RF characterization of junction JJ3, showing both 6 GHz (a,b) and 11 GHz (d,e) measurements and comparison to simulations (c,f). Panels (a) and (d) show some selected IV curves with and without RF power, and theoretical fits using the RSJ model. Panels (b) and (e) show the so called Shapiro map, i.e. the measured dI/dV as a function of both RF power and DC bias current. As a comparison, full Shapiro map simulations are shown in (c) and (f). The best fit parameters were found to be $R_N = 4.8\ \Omega$, $I_c = 17.5\ \mu\text{A}$.

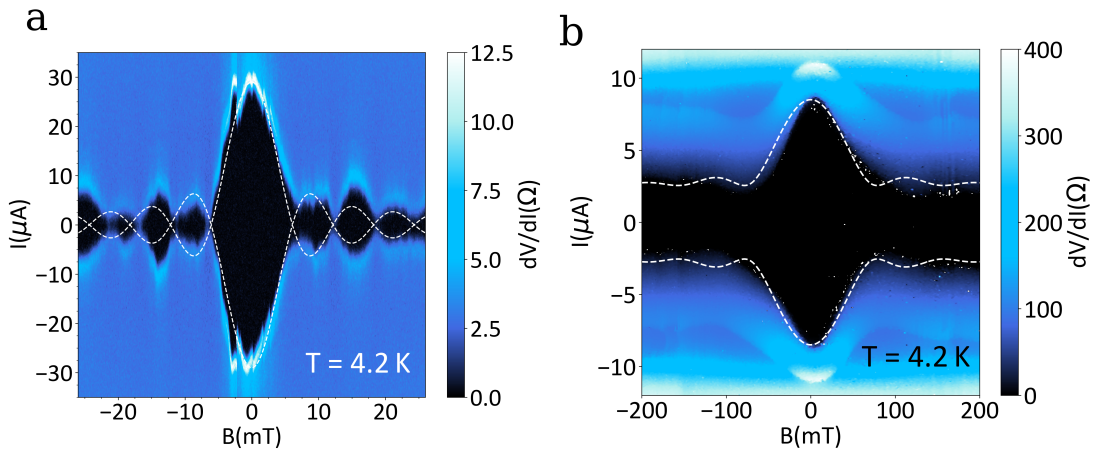


FIG. 5: Panel (a) shows the differential conductance of junction JJ3, measured as a function of magnetic field at 4.2 K with a fit to Eq. 4 (white dotted line). There is clearly a periodic modulation of the critical current as a function of the magnetic field, and at the nodes the critical current vanishes completely. Panel (b) shows the same for junction JJ2, and a fit to Eq. 6. In this junction there is no such clear modulation as a function of magnetic field.

TABLE I: Junction parameters

Name	T_c (K)	t (nm)	w (nm)	Φ (He ⁺ /cm ²)	L_j (nm)	A_j (nm ²)	I_c (μ A)	R_n (Ω)	$I_c R_n$ (mV)	J_c (kA/cm ²)	R_{\square} (Ω)	C(F)
JJ1	13.00	35	860	$9.8 \cdot 10^{18}$	3	30100	2.2	173	0.381	7.31	29.8	$1 \cdot 10^{-17}$
JJ2	15.70	100	300	$1.3 \cdot 10^{19}$	12	30000	9.0	160	1.44	30.0	4.00	$2 \cdot 10^{-15}$
JJ3	13.90	48	2030	$1.1 \cdot 10^{19}$	30	97440	44	4.8	0.211	45.2	0.32	$4 \cdot 10^{-13}$
JJ4	12.84	35	1500	$2.9 \cdot 10^{18}$	14	52500	390	2.5	0.98	743	0.27	$5 \cdot 10^{-14}$

inhomogeneity so that $\gamma^2 = (\bar{I}_1^2/I_0^2) \cdot (1/\pi N)$. When we fitted Eq. 6 to the measured $I_c(B)$ of JJ2, we got a reasonable fit with $\gamma = 0.3$. From Figure 5 (b), we can determine the position of the first minimum, and from this we get $\Delta B \approx 90$ mT. When we use Eq. 4 to calculate the Josephson penetration depth for JJ2 we get 40 ± 20 nm. Hence, the determined λ_j for both junctions are reasonably close to each other, but differ considerably from the literature values as well as the BCS prediction. For JJ2, the Rosenthal correction gives $\Delta B \approx 60$ mT, which is not too far from the measured value and thus might explain the observed node spacing in this case.

CONCLUSIONS

In this study, we have presented for the first time precise local control of superconductivity of NbTiN films using He ion irradiation, and shown that this can be utilized for the fabrication of highly tunable weak links for Josephson junctions. We also extensively characterized the fabricated Josephson junctions using both dc and microwave transport measurements, as well as magnetotransport measurements, and show that the fabricated junctions are of high quality. Additionally, we showed that we are able to tune the barrier strength and fabricate really strong metallic barriers, pushing the limit between metallic and insulating state. The junctions with strongest barrier have excellent thermal stability (weak dependence on temperature) already at 1.5 K, which is quite promising for example for higher temperature quantum information and superconducting electronics applications.

ACKNOWLEDGEMENTS

Authors wish to thank Geng Zhuoran and Pauli Virtanen for discussions and providing parts of the codes, as well as Antti Kanninen for the help with the RF measurements. We also thank Tatu Korkiamäki for the help with some of the cryogenic measurements.

This research was supported by the Academy of Finland project number 341823, the Vilho, Yrjö and Kalle Väisälä Foundation of the Finnish Academy of Science

and Letters and Jenny and Antti Wihuri Foundation.

* email: akperuht@jyu.fi

† maasilta@jyu.fi

- [1] P. Anderson, Theory of dirty superconductors, Journal of Physics and Chemistry of Solids **11**, 26 (1959).
- [2] K. K. Likharev, Superconducting weak links, Rev. Mod. Phys. **51**, 101 (1979).
- [3] S. Cybart, E. Cho, T. Wong, B. Wehlin, M. Ma, C. Huynh, and R. Dynes, Nano josephson superconducting tunnel junctions in YBa₂Cu₃O_{7- σ} directly patterned with a focused helium ion beam, Nature nanotechnology **10**, 598–602 (2015).
- [4] B. Müller, M. Karrer, F. Limberger, M. Becker, B. Schröppel, C. Burkhardt, R. Kleiner, E. Goldobin, and D. Koelle, Josephson junctions and squids created by focused helium-ion-beam irradiation of yba₂cu₃o₇, Phys. Rev. Applied **11**, 044082 (2019).
- [5] H. Li, H. Cai, E. Y. Cho, S. J. McCoy, Y.-T. Wang, J. C. LeFebvre, Y. W. Zhou, and S. A. Cybart, High-transition-temperature nanoscale superconducting quantum interference devices directly written with a focused helium ion beam, Applied Physics Letters **116**, 070601 (2020).
- [6] Z. Chen, Y. Li, R. Zhu, J. Xu, T. Xu, D. Yin, X. Cai, Y. Wang, J. Lu, Y. Zhang, *et al.*, High temperature superconducting yba₂cu₃o_{7- δ} josephson junction fabricated with a focused helium ion beam, Chinese Physics Letters (2022).
- [7] L. Kasaei, T. Melbourne, V. Manichev, L. C. Feldman, T. Gustafsson, K. Chen, X. X. Xi, and B. A. Davidson, MgB₂ josephson junctions produced by focused helium ion beam irradiation, AIP Advances **8**, 075020 (2018).
- [8] Y.-T. Wang, J. C. LeFebvre, E. Y. Cho, S. J. McCoy, H. Li, G. Gu, K. Kadowaki, and S. A. Cybart, Fabrication of Bi₂Sr₂CaCu₂O_{8+x} ab-plane josephson junctions by a focused helium ion beam, IEEE Transactions on Applied Superconductivity **31**, 1 (2021).
- [9] K. Makise, T. Odou, S. Ezaki, T. Asano, and B. Shinozaki, Superconductor–insulator transition in two-dimensional NbN/MgO and NbN/AlN/MgO films, Materials Research Express **2**, 106001 (2015).
- [10] S. Ezaki, K. Makise, B. Shinozaki, T. Odo, T. Asano, H. Terai, T. Yamashita, S. Miki, and Z. Wang, Localization and interaction effects in ultrathin epitaxial NbN superconducting films, Journal of Physics: Condensed Matter **24**, 475702 (2012).

- [11] J. Yong, T. R. Lemberger, L. Benfatto, K. Ilin, and M. Siegel, Robustness of the Berezinskii-Kosterlitz-Thouless transition in ultrathin NbN films near the superconductor-insulator transition, *Phys. Rev. B* **87**, 184505 (2013).
- [12] N. Hadacek, M. Sanquer, and J.-C. Villégier, Double reentrant superconductor-insulator transition in thin TiN films, *Phys. Rev. B* **69**, 024505 (2004).
- [13] T. I. Baturina, C. Strunk, M. R. Baklanov, and A. Satta, Quantum Metallicity on the High-Field Side of the Superconductor-Insulator Transition, *Phys. Rev. Lett.* **98**, 127003 (2007).
- [14] M. V. Burdastyh, S. V. Postolova, T. I. Baturina, T. Proslier, V. M. Vinokur, and A. Y. Mironova, Superconductor-Insulator Transition in NbTiN Films, *JETP LETTERS* **106**, 749–753 (2017).
- [15] M. Burdastyh, S. Postolova, T. Proslier, S. Ustavshikov, A. Antonov, V. Vinokur, and A. Mironov, Superconducting phase transitions in disordered NbTiN films, *Scientific Reports* **10** (2020).
- [16] G. D. Martinez, D. Buckley, I. Charaev, A. Dane, D. E. Dow, and K. K. Berggren, Superconducting nanowire fabrication on niobium nitride using helium ion irradiation (2020).
- [17] A. Ruhtinas, *Direct writing of Josephson junctions in superconducting nitrides with focused helium ion beam*, Master's thesis, University of Jyväskylä (2020).
- [18] T. M. Bretz-Sullivan, R. M. Lewis, A. L. Lima-Sharma, D. Lidsky, C. M. Smyth, C. T. Harris, M. Venuti, S. Eley, and T.-M. Lu, High kinetic inductance nbtin superconducting transmission line resonators in the very thin film limit, *Applied Physics Letters* **121**, 052602 (2022).
- [19] M. Müller, T. Luschmann, A. Faltermeier, S. Weichselbaumer, L. Koch, G. B. P. Huber, H. W. Schumacher, N. Ubbelohde, D. Reifert, T. Scheller, F. Deppe, A. Marx, S. Filipp, M. Althammer, R. Gross, and H. Huebl, Magnetic field robust high quality factor nbtin superconducting microwave resonators, *Materials for Quantum Technology* **2**, 015002 (2022).
- [20] L. Yu, R. Gandikota, R. K. Singh, L. Gu, D. J. Smith, X. Meng, X. Zeng, T. V. Duzer, J. M. Rowell, and N. Newman, Internally shunted josephson junctions with barriers tuned near the metal-insulator transition for rsfq logic applications, *Superconductor Science and Technology* **19**, 719 (2006).
- [21] I. Esmaeil Zadeh, J. W. N. Los, R. B. M. Gourgues, V. Steinmetz, G. Bulgarini, S. M. Dobrovolskiy, V. Zwiller, and S. N. Dorenbos, Single-photon detectors combining high efficiency, high detection rates, and ultra-high timing resolution, *APL Photonics* **2**, 111301 (2017).
- [22] C. Schuck, W. H. P. Pernice, and H. X. Tang, Nbtin superconducting nanowire detectors for visible and telecom wavelengths single photon counting on Si_3N_4 photonic circuits, *Applied Physics Letters* **102**, 051101 (2013).
- [23] S. Shiba, Y. Irimajiri, T. Yamakura, H. Maezawa, N. Sekine, I. Hosako, and S. Yamamoto, 3.1-thz heterodyne receiver using an nbtin hot-electron bolometer mixer and a quantum cascade laser, *IEEE Transactions on Terahertz Science and Technology* **2**, 22 (2012).
- [24] A. Karpov, D. Miller, F. Rice, J. A. Stern, B. Bumble, H. G. LeDuc, and J. Zmuidzinas, Low noise 1 thz–1.4 thz mixers using nb/al-aln/nbtin sis junctions, *IEEE Transactions on Applied Superconductivity* **17**, 343 (2007).
- [25] A. Torgovkin, S. Chaudhuri, A. Ruhtinas, M. Lahtinen, T. Sajavaara, and I. J. Maasilta, High quality superconducting titanium nitride thin film growth using infrared pulsed laser deposition, *Superconductor Science and Technology* **31**, 055017 (2018).
- [26] S. Chaudhuri, I. J. Maasilta, L. Chandernagor, M. Ging, and M. Lahtinen, Fabrication of superconducting tantalum nitride thin films using infrared pulsed laser deposition, *Journal of Vacuum Science & Technology A* **31**, 061502 (2013), <https://doi.org/10.1116/1.4812698>.
- [27] S. Chaudhuri, M. R. Nevala, T. Hakkarainen, T. Niemi, and I. J. Maasilta, Infrared pulsed laser deposition of niobium nitride thin films, *IEEE Transactions on Applied Superconductivity* **21**, 143 (2011).
- [28] L. Pelaz, L. A. Marqués, and J. Barbolla, Ion-beam-induced amorphization and recrystallization in silicon, *Journal of Applied Physics* **96**, 5947 (2004).
- [29] J. Nord, K. Nordlund, and J. Keinonen, Amorphization mechanism and defect structures in ion-beam-amorphized si, ge, and gaas, *Phys. Rev. B* **65**, 165329 (2002).
- [30] M. Tinkham, *Introduction to Superconductivity* (Dover Publications, 2004).
- [31] I. O. Kulik and A. N. Omel'yanchuk, Contribution to the microscopic theory of the josephson effect in superconducting bridges, *JETP Lett. (USSR)* **21**, 96 (1975).
- [32] V. Ambegaokar and A. Baratoff, Tunneling between superconductors, *Phys. Rev. Lett.* **10**, 486 (1963).
- [33] P. Virtanen and T. T. Heikkilä, Thermoelectric effects in superconducting proximity structures, *Appl. Phys. A* **89**, 625 (2007), source code available at <https://gitlab.jyu.fi/jyucmt/usadell>.
- [34] H. Courtois, M. Meschke, J. T. Peltonen, and J. P. Pekola, Origin of hysteresis in a proximity josephson junction, *Phys. Rev. Lett.* **101**, 067002 (2008).
- [35] U. Eckern, G. Schön, and V. Ambegaokar, Quantum dynamics of a superconducting tunnel junction, *Phys. Rev. B* **30**, 6419 (1984).
- [36] A. I. Larkin and Y. N. Ovchinnikov, Decay of the supercurrent in tunnel junctions, *Phys. Rev. B* **28**, 6281 (1983).
- [37] P. A. Rosenthal, M. R. Beasley, K. Char, M. S. Colclough, and G. Zaharchuk, Flux focusing effects in planar thin-film grain-boundary Josephson junctions, *Applied Physics Letters* **59**, 3482 (1991).
- [38] H. J. Suominen, J. Danon, M. Kjaergaard, K. Flensberg, J. Shabani, C. J. Palmstrøm, F. Nichele, and C. M. Marcus, Anomalous fraunhofer interference in epitaxial superconductor-semiconductor josephson junctions, *Phys. Rev. B* **95**, 035307 (2017).
- [39] L. Yu, R. Singh, H. Liu, S. Wu, R. Hu, D. Durand, J. Bulman, J. Rowell, and N. Newman, Fabrication of niobium titanium nitride thin films with high superconducting transition temperatures and short penetration lengths, *Applied Superconductivity, IEEE Transactions on* **15**, 44 (2005).
- [40] H. Yamamori, H. Sasaki, and S. Kohjiro, Preparation of overdamped NbTiN Josephson junctions with bilayered Ti–TiN barriers, *Journal of Applied Physics* **108**, 113904 (2010).
- [41] P. A. Rosenthal, M. R. Beasley, K. Char, M. S. Colclough, and G. Zaharchuk, Effect of fluctuations on the dependence of the Josephson current on magnetic field strength, *Zh. Eksp. Teor. Fiz* **58**, 1497 (1970).